

An observational signature for extremal black holes

Stefanos Aretakis,¹ Gaurav Khanna,^{2,3,4,5} and Subir Sabharwal⁵

¹*Department of Mathematics, University of Toronto,
40 St George Street, Toronto, ON, Canada*

²*Department of Physics, University of Rhode Island, Kingston, RI 02881, USA*

³*Department of Physics, University of Massachusetts Dartmouth,
285 Old Westport Rd., North Dartmouth, MA 02747, USA*

⁴*Center for Scientific Computing & Data-Science Research, University of
Massachusetts Dartmouth, 285 Old Westport Rd., North Dartmouth, MA 02747, USA*

⁵*Center for Computational Research, University of Rhode Island, Kingston, RI 02881, USA*

We consider scalar perturbations of the Reissner–Nordström family and the Kerr family. We derive a characteristic expression of the radiation field, *at any given unit solid angle* of future null infinity, and numerically show that its amplitude gets excited only in the extremal case. Our work, therefore, identifies an observational signature for extremal black holes. Moreover, we show that the source of the excitation is the extremal horizon instability and its magnitude is exactly equal to the conserved horizon charge.

INTRODUCTION

Black holes are one of the most interesting and important predictions of general relativity. In this paper, we study signals that could potentially be received by measurements on Earth leading to the detection of black holes and further understanding of their properties. Specifically, we address the problem of deriving *observational signatures* of black holes, namely the problem of finding distinguishing features of *the dynamics of perturbations of black holes* which can be measured and studied by far-away observers.

In this paper, we focus on observational signatures of a special class of black holes, the so-called *extremal black holes* – specifically extremal Reissner–Nordström (ERN) and extremal Kerr (EK). These black holes play a fundamental role in mathematical relativity, astrophysics and high energy physics. From a theoretical point of view, they saturate geometric inequalities for the mass, angular momentum and charge [1, 11]. Furthermore, they play an important role in the study of Hawking radiation and more generally in quantum gravity [17], and in string theory [20] due to the fact that they have zero temperature. Their near-horizon geometry produces new solutions to the Einstein equations with conformally invariant properties [10]. Both gravitational and electromagnetic signatures of the near-horizon geometry have been introduced in [15, 16]. On the other hand, from a more practical point of view, astronomical evidence suggests that near-extremal black holes are ubiquitous in the universe. Evidence supports the existence of both stellar near-extremal black holes [22] and super-massive near-extremal black holes [8]. Even though, the spins of the astrophysical black holes in all the aforementioned works are below the upper bound

called the Thorne limit [21], recent works open the possibility that there are astrophysical black holes beyond the Thorne limit [19]. *The present work provides an additional tool in the quest of finding black holes that are near or beyond the Thorne limit.*

Perturbations of extremal black holes exhibit a *horizon instability* which manifests itself in the growth along the event horizon of derivatives transversal to the event horizon [4–6, 18]. This dynamical behavior of extremal black holes originates from a characteristic conserved charge along the event horizon, known as the horizon charge $H[\psi]$, where ψ is a scalar perturbation. The existence of this charge calls into question *the no-hair hypothesis* [25–27] for extremal black holes according to which the only externally observable classical parameters of a black hole spacetime are the mass, angular momentum and the electric charge. On the other hand, we note that it has been shown [4] that all translation-invariant quantities decay in time away from the extremal horizon; hence, the conserved charge $H[\psi]$ leaves a non-decaying trace of the perturbation **only** along the horizon and for this reason it can be regarded as *horizon hair*. In other words, *the charge $H[\psi]$ could be viewed as yet another classical parameter of the extremal black hole spacetime.* We remark that the observational signature of the present paper relies precisely on the existence of $H[\psi]$. Our work shows that the horizon hair $H[\psi]$ is classically measurable by external observers, including far-away observers, indeed **falsifying the no-hair hypothesis in the case of extremal black holes.** More specifically, we note that the proposed signature is observable by a single detector at null infinity i.e. a fixed unit solid angle; as opposed to a previously published expression that requires an inte-

gral over the entire S^2 sphere [7].

It is worth noting that the same notion of horizon hair $H[\psi]$ approximately applies in the case of near extremal black holes, as a *transient* with duration dependent on the proximity to extremality [12]. Therefore, we expect the results of this work to similarly hold in the near extremal cases. We also remark that, under the presence of superradiance, an amplified version [9, 13] of the horizon instability on such backgrounds due to the existence a sequence of zero-damped quasinormal modes is already known [14, 23].

THE GEOMETRIC SETTING

Our goal is the measurement of the horizon hair $H[\psi]$ by far-away observers who receive radiation from the near-horizon region. In our model, observers are assumed to live on null generators of the future null infinity \mathcal{I}^+ of either the Reissner–Nordström family or the Kerr family. The future null infinity \mathcal{I}^+ admits the following coordinates

$$\mathcal{I}^+ = (\tau, \vartheta),$$

where the coordinates are defined as follows

- τ : the *retarded time* which represents the local time of any given ideal observer at \mathcal{I}^+ ,
- $\vartheta = (\theta^1, \theta^2)$: the *unit solid angle* which represents the direction of any given ideal observer along \mathcal{I}^+ .

Null generators of \mathcal{I}^+ are parametrized by

$$\{(\tau, \vartheta_0), \tau \in \mathbb{R}\}$$

where ϑ_0 is a fixed unit solid angle.

OBSERVATIONAL SIGNATURES IN BOUNDED REGIONS

We consider massless scalar perturbations ψ on either the Reissner–Nordström (RN) family or the Kerr family:

$$\square_g \psi = 0 \quad (1)$$

where g is the RN/Kerr metric. Observational signatures can easily be derived in bounded regions from known results. Starting first from the event horizon, recall [3] that asymptotically as $\tau \rightarrow \infty$ we have

$$\psi|_{\mathcal{H}^+}(\tau, \vartheta) \sim \begin{cases} 8I^{(1)}[\psi] \cdot \frac{1}{\tau^3} & \text{on subextremal RN} \\ \frac{2}{M} H[\psi] \cdot \frac{1}{\tau} & \text{on ERN} \end{cases}$$

where $H[\psi]$ is defined below,

$$H[\psi] := -\frac{M^2}{4\pi} \int_{\text{EH}} \partial_r(r\psi) d\Omega \quad (2)$$

and $I^{(1)}[\psi]$ is defined in the following section. Defining the signature $s_{\mathcal{H}^+}(\vartheta)$ as follows

$$s_{\mathcal{H}^+}(\vartheta) = \lim_{\tau \rightarrow \infty} \frac{M}{2} \tau \cdot \psi|_{\mathcal{H}^+}(\tau, \vartheta) \quad (3)$$

then

$$s_{\mathcal{H}^+}(\vartheta) = \begin{cases} 0 & \text{for subextremal RN} \\ H[\psi] & \text{for ERN} \end{cases}$$

We next consider the constant r hypersurface $R_{r_0} = \{r = r_0\}$. From [3] it follows that asymptotically along R_{r_0} we have

$$\psi|_{\{r=r_0\}}(\tau, \vartheta) \sim \begin{cases} 8I^{(1)}[\psi] \cdot \frac{1}{\tau^3} & \text{on subextremal RN} \\ \frac{4MH}{r_0 - M} \cdot \frac{1}{\tau^2} & \text{on ERN} \end{cases}$$

Defining the signature $s_{r_0}(\vartheta)$ as follows

$$s_{r_0}(\vartheta) = \lim_{\tau \rightarrow \infty} \frac{r_0 - M}{4M} \tau^2 \cdot \psi|_{\{r=r_0\}}(\tau, \vartheta) \quad (4)$$

then

$$s_{r_0}(\vartheta) = \begin{cases} 0 & \text{for subextremal RN} \\ H[\psi] & \text{for ERN} \end{cases}$$

THE OBSERVATIONAL SIGNATURE $s_{\mathcal{I}^+}(\vartheta)$ AT NULL INFINITY

Define the radiation field Ψ of the scalar field ψ as follows

$$\Psi(\tau, \vartheta) = \lim_{r \rightarrow \infty} (r\psi)(\tau, r, \vartheta).$$

We then define the following limits

$$C_1(\vartheta) = \lim_{\tau \rightarrow \infty} \tau^2 \cdot \Psi(\tau, \vartheta) \quad (5)$$

and

$$C_2(\vartheta) = \lim_{\tau \rightarrow \infty} \frac{\tau}{\log(\tau/M)} \cdot (\tau^2 \cdot \Psi(\tau, \vartheta) - C_1(\vartheta)). \quad (6)$$

Clearly, both $C_1(\vartheta), C_2(\vartheta)$ can be computed by knowing the radiation field $\Psi(\tau, \vartheta)$ along a fixed null generator of null infinity corresponding to the solid angle ϑ . The following asymptotic expansion follows then for the radiation field:

$$\Psi(\tau, \vartheta) = C_1(\vartheta) \frac{1}{\tau^2} + C_2(\vartheta) \frac{\log(\tau/M)}{\tau^3} + O\left(\frac{1}{\tau^3}\right).$$

In the sub-extremal case, it has been known [2] that

$$C_1(\vartheta) = -2I^{(1)}, \quad C_2(\vartheta) = 8MI^{(1)} \quad (7)$$

where $I^{(1)} = I^{(1)}[\psi]$ is given in terms of the initial data of ψ by the following expression

$$I^{(1)}[\psi] = \frac{M}{4\pi} \int_{\Sigma_0 \cap \mathcal{H}^+} \psi + \frac{M}{4\pi} \int_{\Sigma_0} \nabla \psi \cdot n_{\Sigma_0}$$

where the above integrals are taken relative to the respective volume forms. An alternative formula [24] for $I^{(1)}$ allows its computation from future null infinity as follows

$$I^{(1)}[\psi] = \frac{M}{4\pi} \int_{\mathcal{I}^+ \cap \{\tau \geq 0\}} \Psi(\tau, \vartheta) d\vartheta d\tau. \quad (8)$$

Note in order to compute $I^{(1)}[\psi]$ via (8) we need to integrate the radiation field $\Psi(\tau, \vartheta)$ over all solid angles ϑ . Hence formula (8) does **not** provide an anisotropic measurement of $I^{(1)}[\psi]$. It is important however to note that for the full sub-extremal RN family we have $C_2(\vartheta)/C_1(\vartheta) = -4M$ and this ratio is independent of ψ or ϑ .

Switching now to the extremal RN spacetimes, previous work [3] has shown that

$$C_1(\vartheta) = 4MH - 2I^{(1)} \quad (9)$$

One of the numerical results of the present paper is the following expression for $C_2(\vartheta)$ in extremal RN:

$$C_2(\vartheta) = -32M^2H + 8MI^{(1)} \quad (10)$$

for all angles ϑ . The relations (9) and (10) imply that

$$H[\psi] = -\frac{1}{16M^2} (C_2(\vartheta) + 4MC_1(\vartheta)) \quad (11)$$

This motivates the following definition for extremal RN

$$s_{\mathcal{I}^+}(\vartheta) = -\frac{1}{16M^2} (C_2(\vartheta) + 4MC_1(\vartheta)) \quad (12)$$

or, equivalently,

$$s_{\mathcal{I}^+}(\vartheta) = -\frac{1}{16M^2} \cdot \lim_{\tau \rightarrow \infty} \left[4M\tau^2 \cdot \Psi(\tau, \vartheta) - \frac{\tau}{\log(\tau/M)} \cdot \left(\lim_{\tau \rightarrow \infty} \tau^2 \cdot \Psi(\tau, \vartheta) \right) + \frac{\tau^3}{\log(\tau/M)} \Psi(\tau, \vartheta) \right] \quad (13)$$

and notice that

$$s_{\mathcal{I}^+}(\vartheta) = \begin{cases} 0 & \text{for subextremal RN} \\ H[\psi] & \text{for ERN} \end{cases}$$

The signature $s_{\mathcal{I}^+}(\vartheta)$ allows us to differentiate extremality from sub-extremality and in fact to compute (in the extremal case) the horizon hair $H[\psi]$ by knowing the radiation field along a fixed null generator of \mathcal{I}^+ .

Remark. *Our analysis relies on the fact that for the full sub-extremal RN we have $\frac{C_2(\vartheta)}{C_1(\vartheta)} = -4M$. Given therefore the expression $C_1(\vartheta) = 4MH - 2I^{(1)}$ the worst-case scenario would have been that in extremal RN: $C_2(\vartheta) = -16M^2H + 8MI^{(1)}$.*

We can even compute $I^{(1)}$ in a similar fashion:

$$I^{(1)}[\psi] = -\left(C_1(\vartheta) + \frac{1}{8M} C_2(\vartheta) \right) \quad (14)$$

NUMERICAL APPROACH & RESULTS

In this section we summarize our numerical approach and present detailed numerical evidence for the fact that $s_{\mathcal{I}^+}(\vartheta)$ equals $H[\psi]$ both the ERN and EK cases, and zero for the sub-extremal cases.

Numerical Methodology

We solve the scalar wave equation for perturbations in ERN and EK black hole backgrounds, focusing on axisymmetric modes ($m = 0$). We modify the equation to work in compactified hyperboloidal coordinates $(\tau, \rho, \theta^1, \theta^2)$ that allow for time evolution on hypersurfaces which bring \mathcal{I}^+ to a finite radial coordinate $\rho(\mathcal{I}^+) = S < \infty$. The relationship between these new coordinates (τ, ρ) and the spherical Boyer-Lindquist coordi-

nates (t, r) is [28]

$$\begin{aligned}\Omega &= 1 - \frac{\rho}{S} \\ r &= \frac{\rho}{\Omega(\rho)} \\ v \equiv t + r_* - r &= \tau + \frac{\rho}{\Omega(\rho)} - \rho - 4M \log \Omega(\rho)\end{aligned}\quad (15)$$

where S denotes the location of \mathcal{I}^+ in hyperboloidal coordinates, r_* is the usual tortoise coordinate and v is the modified advanced time. Note that the angular variables are the same in both coordinate systems.

Our numerical implementation scheme entails re-writing the second order PDE in terms of two coupled first-order differential equations. We solve this system using a high-order weighted essentially non-oscillatory (WENO) finite-difference scheme with explicit Shu-Osher time-stepping. In the RN case, we solve a (1+1)D system using the standard decomposition in spherical harmonics, while in the Kerr case we solve (2+1)D system. Details may be found in our previous work [12, 29–32]. We choose $S = 19.0$ and the location of \mathcal{H}^+ such that, $\rho(\mathcal{H}^+) = 0.95$. The initial data is a truncated Gaussian centered at $\rho = (1.0, 1.1, 1.2)$ with a width of $(0.16, 0.22, 0.32)$ and non-zero for $\rho \in [0.95, 8]$. This ensures compactly supported initial data but with non-zero support on the \mathcal{H}^+ surface. The angular distribution of this initial data is spherically symmetric i.e. the $\ell = 0$ monopole. The initial data’s angular distribution can be considered as “generic” i.e. includes all axisymmetric multipoles, since the higher-multipoles decay rapidly leaving the $\ell = 0$ monopole to dominate at late times.

Finally, to complete these long duration, high-accuracy and high-precision computations in a reasonable time-frame we make extensive use GPGPU-based parallel computing. For additional details on implementation of such intensive computations on a parallel GPU architecture, we refer the reader to our earlier work on the subject [29]. Note that these simulations take significant computational resources to run. Each RN simulations takes a week of wall-clock time, while the Kerr ones take a month. For this reason, we focused our efforts on the extremal cases and did not attempt any near-extremal cases. However, our previous work [12] in that context suggests that for cases in which the black holes are very close to extremality, the extremal case results are a good approximation as a “transient” i.e. for early times.

Numerical Results

The numerical solution of the Teukolsky equation in compactified coordinates allows us to study the time evolution of the field at \mathcal{I}^+ with $\theta^{1,2} = \pi/2$. To calculate $s_{\mathcal{I}^+}(\vartheta)$ for subextremal RN, we first calculate the *local power index* (LPI) defined as $LPI \equiv \tau \dot{\psi} / \psi$ at each moment in time for $\tau/M \gtrsim 3300$. This is because under the assumptions of the previous sections for the field expansion at \mathcal{I}^+ , the LPI is related to the ratio $C_2(\vartheta)/C_1(\vartheta)$ as

$$\begin{aligned}\tau \left[\frac{\tau \dot{\psi}}{\psi} + 2 \right] &= -\frac{C_2(\vartheta)}{C_1(\vartheta)} \log(\tau/M) + \frac{C_2(\vartheta)}{C_1(\vartheta)} \\ &+ \mathcal{O} \left(M^2 \frac{\log(\tau/M)}{\tau} \right) + \dots\end{aligned}\quad (16)$$

Thus, the *LPI* gives us a direct probe of the ratio $C_2(\vartheta)/C_1(\vartheta)$ by regressing $\tau \times (LPI + 2)$ against $\log(\tau/M)$. However, since the *LPI* requires time derivatives of the field, the regression coefficient (which should theoretically equal $C_2(\vartheta)/C_1(\vartheta)$) as a function of time is noisy. To smooth the time evolution of the estimated ratio $C_2(\vartheta)/C_1(\vartheta)$, we use a smoothing algorithm that employs a simple moving average but with variable window size. Specifically, the algorithm assigns a dynamical window for the moving average which minimizes the variance (a measure of roughness of first order differences of the input time series) while preserving its kurtosis (a measure of tailedness). In Fig 1, we plot the estimated values of $s_{\mathcal{I}^+}(\vartheta)$ against time for three different subextremal RN cases, $Q/M = [0.3, 0.4, 0.5]$ at late times ($\tau/M \gtrsim 3300$). In each of these cases, it’s clear from the numerical data that $s_{\mathcal{I}^+}(\vartheta)$ asymptotes to 0 at late times as expected from the earlier sections. This implies that for subextremal BHs, irrespective of their deviation from extremality, $C_2(\vartheta) = -4MC_1(\vartheta)$ as expected. Our proposal is that the quantity $s_{\mathcal{I}^+}(\vartheta)$ which depends on the sub-leading terms in the dynamics of the radiation field at \mathcal{I}^+ can indeed provide a signature for extremality. In order to demonstrate this, we determine $s_{\mathcal{I}^+}(\vartheta)$ for extremal BHs with different initial conditions and plot it against their respective constant, $H[\psi]$ that depends on initial conditions.

To see the effect of sub-leading terms in the tail behavior for extremal BHs, the simulations were performed up to very late times ($t/M = 8000$). Since at each step in the time evolution, we accumulate numerical error in the form of truncation of derivatives, we find that the numerical procedure employed above for sub-extremal BHs didn’t

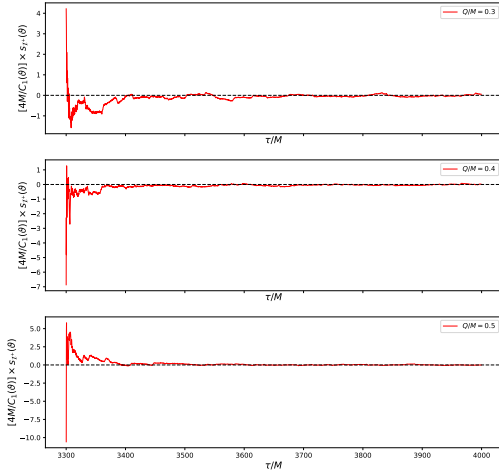


Figure 1. Time evolution of $[4M/C_1(\vartheta)] \times s_{\mathcal{I}^+}(\vartheta)$ for three sub-extremal RNs, $Q/M = [0.3, 0.4, 0.5]$ for any value of ϑ . Note that $s_{\mathcal{I}^+}(\vartheta)$ asymptotes to 0 as we evolve the scalar field at \mathcal{I}^+ .

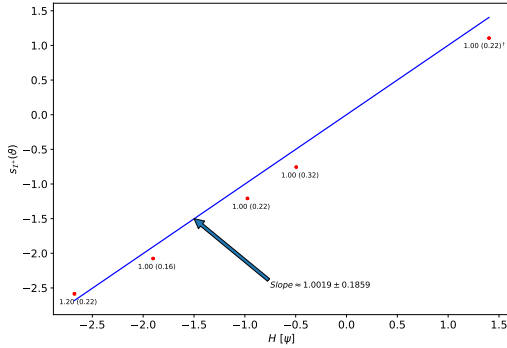


Figure 2. Best-fit line demonstrating a linear relationship between the horizon constant $H[\psi]$ and the asymptotically extracted $s_{\mathcal{I}^+}(\vartheta)$ for any ϑ for extremal RN. The slope of the best fit-line is 1.0019 ± 0.19 . Each data point is labelled by the initial data used for that computation i.e. the location and width of the Gaussian pulse^a. The Levenberg–Marquardt fitting errors in each data point are too small to be visible on the scale of the plot.

^a The far left data point labelled by the dagger symbol uses initial data in which the field is zero while the momentum is set to the Gaussian pulse.

work very well for the extremal case – specifically the *LPI* was very noisy for the extremal case. Instead, we determined $C_1(\vartheta)$ and $C_2(\vartheta)$ at \mathcal{I}^+ from the time series of the scalar field at \mathcal{I}^+ at late times ($\tau/M \gtrsim 5000$) via curve-fitting

using the Levenberg–Marquardt algorithm. We plot the relationship between $s_{\mathcal{I}^+}(\vartheta)$ and $H[\psi]$ in Fig 2 which clearly implies a linear relationship with a slope of the best-fit line being ≈ 1 as expected. Note that we include the origin $(0, 0)$ as a constraint in our linear fitting since $s_{\mathcal{I}^+}(\vartheta)$ must go to zero when $H[\psi] = 0$ (see the Appendix).

Finally, we repeated the same analysis for Kerr black holes with axisymmetric scalar perturbations ($m = 0$) focusing only on the dominant excitation mode ($l = 0$). To start, in Fig 3, we plot the estimated values of $s_{\mathcal{I}^+}(\vartheta)$ against time for three different subextremal Kerr cases, $a/M = [0.3, 0.4, 0.5]$ at late times ($\tau/M \gtrsim 3300$). In each of these cases, it’s clear from the numerical data that $s_{\mathcal{I}^+}(\vartheta)$ asymptotes to 0 at late times. For the extremal Kerr case, we find a

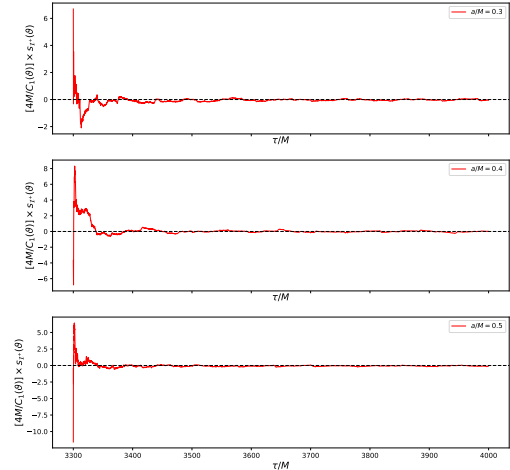


Figure 3. Time evolution of $[4M/C_1(\vartheta)] \times s_{\mathcal{I}^+}(\vartheta)$ for three sub-extremal Kerr cases, $a/M = [0.3, 0.4, 0.5]$ for any value of ϑ . Note that $s_{\mathcal{I}^+}(\vartheta)$ asymptotes to 0 as we evolve the scalar field at \mathcal{I}^+ .

linear relationship between $s_{\mathcal{I}^+}$ (redefined below with an extra $1/4$ compared to the ERN case) vs $H[\psi]$ where the quantities are defined similar to RN black holes, i.e. in terms of $C_1(\vartheta)$ and $C_2(\vartheta)$. We present the results for EK in Fig 4. Note that $s_{\mathcal{I}^+}$ is redefined for Kerr with an overall $1/4$ compared to (12),

$$s_{\mathcal{I}^+}^K(\vartheta) = -\frac{1}{64M^2} (C_2(\vartheta) + 4MC_1(\vartheta)) \quad (17)$$

or equivalently,

$$s_{\mathcal{I}^+}^K(\vartheta) = -\frac{1}{64M^2} \cdot \lim_{\tau \rightarrow \infty} \left[4M\tau^2 \cdot \Psi(\tau, \vartheta) - \frac{\tau}{\log(\tau/M)} \cdot \left(\lim_{\tau \rightarrow \infty} \tau^2 \cdot \Psi(\tau, \vartheta) \right) + \frac{\tau^3}{\log(\tau/M)} \Psi(\tau, \vartheta) \right]. \quad (18)$$

This redefinition preserves the property that $s_{\mathcal{I}^+}^K = H[\psi] \neq 0$ for EK but $s_{\mathcal{I}^+}^K = 0$ for sub-extremal Kerr.

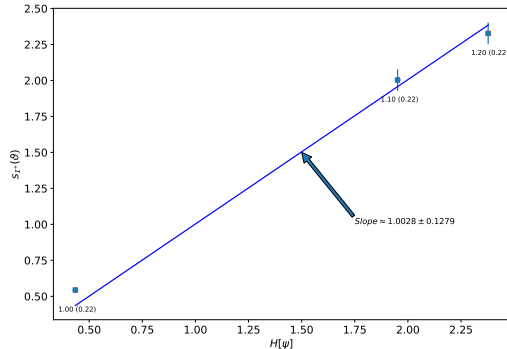


Figure 4. Best-fit line demonstrating a linear relationship between the horizon constant H and the asymptotically extracted $s_{\mathcal{I}^+}^K(\vartheta)$ with $\theta^{1,2} = \pi/2$ for extremal Kerr black holes. The slope of the best fit line is 1.0028 ± 0.13 . Each data point is labelled by the initial data used for that computation i.e. the location and width of the Gaussian pulse. The Levenberg–Marquardt fitting errors are depicted by the vertical bars on each data point.

CONCLUSION

In this paper, we have investigated scalar perturbations of the Reissner–Nordström family and the Kerr family of black holes. Our numerical analysis has allowed us to derive a characteristic excitation for the radiation field at any given unit solid angle of future null infinity. The derived expression is non-zero only in the extremal case, where the black hole’s charge or angular momentum reaches its maximum value. This observation serves as an important observational signature for extremal black holes, distinguishing them from sub-extremal ones.

Furthermore, we have identified the extremal horizon instability as the source of this excitation in the radiation field. Remarkably, we have demonstrated that the magnitude of the excitation in the radiation field precisely matches the conserved horizon charge of the black hole. This shows that the horizon charge is classically measurable by external observers, including far-away observers, thus falsifying the no-hair hypothesis

in the case of extremal black holes.

Our research advances the field of black hole astrophysics by unveiling the observational consequences of extremal black holes and establishing a direct link between the excitation in the radiation field and the conserved horizon charge. These results pave the way for further investigations into the nature and behavior of extremal black holes, opening up new avenues for studying the rich physics associated with these extreme gravitational objects.

ACKNOWLEDGEMENTS

The authors wish to thank Som Bishoyi for finding some errors in the formulae presented and double-checking our numerical work. The original manuscript also benefited from the journal peer-review process. G.K. acknowledges support from NSF Grants No. PHY-2307236 and DMS-2309609. Simulations were performed on the UMass-URI UNITY supercomputer and MIT SuperCloud supported by the Massachusetts Green High Performance Computing Center (MGHPCC). S.A. acknowledge support from the NSERC grant and the Ontario Early Researcher Award.

Appendix: Initial data with no support on the horizon

In this appendix, we show numerical results that offer numerical confirmation that the proposed signature $s_{\mathcal{I}^+}$ works correctly with the initial data lacks support on the horizon for both ERN and EK cases. In Fig. 5 we show a plot of $s_{\mathcal{I}^+}$ for both ERN and EK for an initial Gaussian centered at $\rho = 4.0$ with width 0.22 and truncated outside the window $[1.0, 8.0]$. As mentioned previously, the horizon is located at $\rho = 0.95$ and thus this data has no support on the horizon. It is clear that the signature $s_{\mathcal{I}^+}(\vartheta)$ asymptotes to 0 as we evolve the scalar field. The computational methodology for this Fig. 5 is the same as that used for Fig. 1.

[1] ALAEE, A., KHURI, M., AND KUNDURI, H. Mass-angular momentum inequality for black

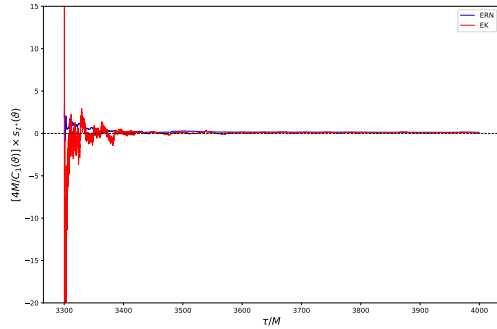


Figure 5. Time evolution of $[4M/C_1(\vartheta)] \times s_{\mathcal{I}^+}(\vartheta)$ for ERN and EK for initial data with no support on the horizon. Note that $s_{\mathcal{I}^+}(\vartheta)$ asymptotes to 0 as we evolve the scalar field at \mathcal{I}^+ .

- ring spacetimes. *Phys. Rev. Lett.* **119** (2017), 071101.
- [2] ANGELOPOULOS, Y., ARETAKIS, S., AND GAJIC, D. Logarithmic corrections in the asymptotic expansion for the radiation field along null infinity. *Journal of Hyperbolic Differential Equations* **16**, 01 (2019), 1–34.
- [3] ANGELOPOULOS, Y., ARETAKIS, S., AND GAJIC, D. Late-time asymptotics for the wave equation on extremal Reissner–Nordström backgrounds. *Advances in Mathematics* **375** (2020).
- [4] ARETAKIS, S. Stability and instability of extreme Reissner–Nordström black hole spacetimes for linear scalar perturbations I. *Commun. Math. Phys.* **307** (2011), 17–63.
- [5] ARETAKIS, S. Stability and instability of extreme Reissner–Nordström black hole spacetimes for linear scalar perturbations II. *Ann. Henri Poincaré* **12** (2011), 1491–1538.
- [6] ARETAKIS, S. Horizon instability of extremal black holes. *Adv. Theor. Math. Phys.* **19** (2015), 507–530.
- [7] ANGELOPOULOS, Y. AND ARETAKIS, S. AND GAJIC, D. Horizon Hair of Extremal Black Holes and Measurements at Null Infinity. *Phys. Rev. Lett.* **121** (2018), 131102.
- [8] BRENNEMAN, L. ET AL. The spin of the supermassive black hole in NGC 3783. *Astrophys. J.* **736**, 103 (2011).
- [9] CASALS, M., GRALLA, S. E., AND ZIMMERMAN, P. Horizon instability of extremal Kerr black holes: Nonaxisymmetric modes and enhanced growth rate. *Phys. Rev. D* **94** (2016), 064003.
- [10] CLAUS, P., DERIX, M., KALLOSH, R., KUMAR, J., TOWNSEND, P. K., AND VAN PROEYEN, A. Black holes and superconformal mechanics. *Phys. Rev. Lett.* **81** (1998), 4553–4556.
- [11] DAIN, S. Angular-momentum–mass inequality for axisymmetric black holes. *Phys. Rev. Lett.* **96** (2006), 101101.
- [12] BURKO, L.M., KHANNA, G. AND SABHARWAL, S. (Transient) Scalar Hair for (Nearly) Extreme Black Holes *Phys. Rev. Research* **1** (2019), 033106.
- [13] GAJIC, D. Azimuthal instabilities on extremal kerr. *arXiv:2302.06636* (2023).
- [14] GLAMPEDAKIS, K., AND ANDERSSON, N. Late-time dynamics of rapidly rotating black holes. *Phys. Rev. D* **64** (2001), 104021.
- [15] GRALLA, S. E., HUGHES, S. A., AND WARBURTON, N. Inspiral into gargantua. *Class. and Quantum Grav.* **33**, 155002 (2016).
- [16] GRALLA, S. E., LUPSASCA, A., AND STROMINGER, A. Observational signature of high spin at the event horizon telescope. *Mon. Not. R. Astron. Soc.* **475**, 3 (2018), 3829–3853.
- [17] HAWKING, S. W., HOROWITZ, G. T., AND ROSS, S. F. Entropy, area, and black hole pairs. *Phys. Rev. D* **51** (1995), 4302–4314.
- [18] LUCIETTI, J., AND REALL, H. S. Gravitational instability of an extreme Kerr black hole. *Phys. Rev. D* **86** (2012), 104030.
- [19] SKADOWSKI, A., BURSA, M., ABRAMOWICZ, M., KLUŻNIAK, W., LASOTA, J.-P., MODERSKI, R., AND SAFARZADEH, M. Spinning up black holes with super-critical accretion flows. *A & A* **532**, A41 (2011).
- [20] STROMINGER, A., AND VAFA, C. Microscopic origin of the Bekenstein–Hawking entropy. *Phys. Lett. B* **379** (1996), 99–104.
- [21] THORNE, K. S. Disk-accretion onto a black hole. ii. evolution of the hole. *Astrophys. J.* **191** (1974), 507–520.
- [22] VOLONTERI, M., MADAU, P., QUATAERT, E., AND REES, M. The distribution and cosmic evolution of massive black hole spins. *Astrophys. J.* **620** (2005), 69–77.
- [23] YANG, H., ZIMMERMAN, A., ZENGINOGLU, A., ZHANG, F., BERTI, E., AND CHEN, Y. Quasinormal modes of nearly extremal Kerr spacetimes: Spectrum bifurcation and power-law ringdown. *Phys. Rev. D* **88** (2013), 044047.
- [24] ANGELOPOULOS, Y., ARETAKIS, S. AND GAJIC, D. Late-time asymptotics for the wave equation on extremal Reissner–Nordström backgrounds *Advances in Mathematics* **375** (2020), 107363.
- [25] BEKENSTEIN, J. D. Late-time asymptotics for the wave equation on extremal Reissner–Nordström backgrounds *Phys. Rev. Lett.* **28** (1972) 452.
- [26] BEKENSTEIN, J. D. Nonexistence of Baryon Number for Black Holes. I *Phys. Rev. D* **5** (1972) 1239.
- [27] BEKENSTEIN, J. D. Nonexistence of Baryon Number for Black Holes. II *Phys. Rev. D* **5** (1972) 2403.
- [28] ZENGINOGLU, A. Hyperboloidal foliations and scri-fixing. *Class. Quantum Grav.* **25** (2008), 145002.
- [29] FIELD, S.E., GOTTLIEB, S., GRANT, Z.J., ISHERWOOD, L.F., AND KHANNA, G. A GPU-Accelerated Mixed-Precision WENO Method for Extremal Black Hole and Gravitational Wave Physics Computations. *Communications on Applied Mathematics and Computation* **5** (2023), 97.
- [30] BURKO, L.M., KHANNA, G. AND SABHARWAL,

- S. Scalar and gravitational hair for extreme Kerr black holes. *Phys. Rev. D* *103* (2021), L021502.
- [31] BURKO, L.M., KHANNA, G. AND SABHARWAL, S. Aretakis Hair for Extreme Kerr Black Holes with Axisymmetric Scalar Perturbations. *Phys. Rev. D* *107* (2023), 124023.
- [32] BURKO, L.M., KHANNA, G. AND SABHARWAL, S. Aretakis Hair for Extreme Kerr Black Holes with Axisymmetric Scalar Perturbations. *Phys. Rev. D* *107* (2023), 124023.